The Early Steps in the Unfolding of Azurin[†]

Bruno Rizzuti,[‡] Valerie Daggett,[§] Rita Guzzi,*[,‡] and Luigi Sportelli[‡]

Dipartimento di Fisica and Unità INFM, Laboratorio di Biofisica Molecolare, Università della Calabria, 87030 Rende CS, Italy, and Department of Medicinal Chemistry, University of Washington, Seattle, Washington 98195-7610

Received June 24, 2004; Revised Manuscript Received September 29, 2004

ABSTRACT: High-temperature molecular dynamics simulations were used to gain insight into the early steps in the unfolding pathway of azurin, a blue copper protein with a β-barrel structure formed by two sheets arranged in a Greek key folding topology. The results reveal that unfolding of the β-barrel in azurin is associated with dislocation of its unique α-helix with respect to the protein scaffold. Exposure of the hydrophobic core to solvent precedes complete disruption of secondary and tertiary structure, and modifications in the region around the active site are directly connected with this event. Denaturation of the protein initiates from the sheet coordinating the copper ion, and the other sheet maintains its topology. Results derived from the simulation were compared with experimental data obtained with different techniques, showing excellent agreement and providing a framework to understand the process of disruption and formation of the β-barrel in azurin.

Understanding the process of protein folding is one of the most challenging questions in structural biology. Details of the mechanism appear to be elusive particularly for β-sheet proteins, because the interactions that stabilize the structure are predominantly nonlocal in nature. Insights into the folding/unfolding reaction can be obtained by employing a combination of numerous experimental techniques (*1*−*3*), as well as using theoretical methods.

Molecular dynamics (MD)[1] is the most realistic simulation technique available, as it allows us to take into account the detailed interactions between all of the protein and solvent atoms. Although the time scale (10 μs to seconds) of protein folding is not yet, or only barely, accessible with the current computer power (*4*), MD is a useful tool for investigating unfolding events (*5*). Results obtained on the engrailed homeodomain (*6*, *7*), WW domain (*8*), and chymotrypsin inhibitor 2 (*9*) have revealed that simulations at high temperature accelerate the unfolding process without affecting the overall pathway. Therefore, integrating MD simulations and experimental studies can enhance our knowledge of the folding process.

Azurin is a blue copper protein (*10*), and it is a good model for studying the thermal unfolding of a β-sheet protein. It is small (128 amino acid residues) and has a β-barrel structure (Figure 1a) arranged in two sheets with a distinctive Greek key folding topology (Figure 1b); a short (13 residue) helix is also present. The temperature of denaturation, or T_m, is 80 °C (*11*). Copper ion in the active site and a single tryptophan residue in the hydrophobic core constitute natural probes that can be used in experiments to monitor structural changes of the protein during unfolding.

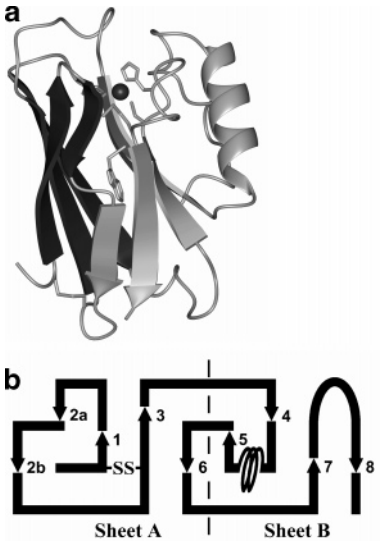

FIGURE 1: (a) Ribbon representation of azurin with the two β-sheets in different colors. Side chains are explicitly shown for copper ligands (top), the tryptophan residue (center), and the disulfide bridge (left bottom). (b) Greek key folding motif of azurin. Strand 2 is split up into 2a (belonging to sheet A) and 2b (sheet B). The latter faces strand 8, closing the β-barrel. The disulfide bridge and the α-helix region (which includes the loops that connect the helix to the β-barrel) are also indicated.

MD simulations have already been performed (*12*−*14*) to study the conformational behavior and the dynamics of azurin at room temperature. Our results (*14*, *15*) have shown a good correspondence between simulation and both crystallographic (*16*) and NMR data (*17*−*19*), and we have evidence for the existence of correlated motions between regions of the protein that are critical for maintaining the structure features and function of this protein.

[†] Financial support for the computational studies was provided by the National Institutes of Health (Grant GM50789 to V.D.). B.R. acknowledges a fellowship from Regione Calabria.

* To whom correspondence should be addressed. Tel: +39-0984-496077. Fax: +39-0984-494401. E-mail: guzzi@fis.unical.it.

[‡] Dipartimento di Fisica and Unità INFM, Università della Calabria.

[§] Department of Medicinal Chemistry, University of Washington.

[1] Abbreviations: MD, molecular dynamics; HB, hydrogen bond; RMSD, root mean square deviation; SASA, solvent-accessible surface area; CD, circular dichroism; DSC, differential scanning calorimetry; EPR, electron paramagnetic resonance; OD, optical density.

10.1021/bi048685t CCC: $27.50
Published on Web 11/17/2004

In this paper, we use high-temperature MD simulations to study the process of thermal unfolding of azurin. In particular, we concentrated our attention on the early events of the unfolding process, to compare our simulation data with the experimental results currently available on azurin (a thorough analysis of the latest steps of the process, i.e., of the unfolded state of azurin, will be presented in a forthcoming paper). This work showed that the succession of the unfolding events, occurring as a function of the simulation time, is fully consistent with the initial part of the experimental unfolding pathway, which is outlined on the basis of the results that some of us (L. Sportelli and R. Guzzi) have obtained on azurin over the past decade. A model is proposed in which the disruption of the β-barrel starts from the β-strands that coordinate the copper ion in a region close to the α-helix and distant from the active site.

MATERIALS AND METHODS

Molecular Dynamics Simulations. MD simulations were performed using an in-house version of the program ENCAD (*20*), and the force field parameters and protocols have been described (*21*, *22*). An all-atom representation was employed for both the protein and solvent. The crystal structure (*16*) of azurin (4AZU entry in the Protein Data Bank) was used as the starting structure for the simulations. Side chain protonation states were adapted to mimic neutral pH, with Asp and Glu residues negatively charged and Arg, Lys, and His positively charged. In particular, His46 and His117 were protonated at N^{ϵ}, since the N^{δ} atoms are metal ligands. The coordination of the Cu ion in the thermal unfolded state of azurin is still not clear, though some hypotheses have been suggested under aerobic conditions (*11*, *23*). In the absence of molecular oxygen, which corresponds to the simulation condition in molecular dynamics, no assignment of the Cu ligands in the unfolded state has been made (*23*). However, experiment clearly indicates that three ligand atoms, S_{Cys112}, N_{His117} and S_{Met121}, comprise the coordination triad in the chemically unfolded state of azurin (*24*−*26*). Thus, this reference model was adopted, and the Cu atom was attached to the three ligands by constraining the bonds to their crystallographic values. Strong charge transfer between Cu and S_{Cys112} (*27*) was modeled by setting a partial charge of +0.5 e on the metal ion and −0.5 e on the (deprotonated) sulfur atom (*12*). The following van der Waals parameters were used for Cu: atomic radius $r_0 = 0.128$ nm and a Lennard-Jones energy minimum of 0.21 kJ·mol^{-1} at $r = 0.24$ nm.

Residual strain in the crystal structure was relieved by 500 cycles of conjugate gradient minimization performed in vacuo. The protein was then solvated in a triclinic box extending at least 0.8 nm in all directions, resulting in a fully hydrated system containing 3621 water molecules. Periodic boundary conditions were employed to avoid edge effects. The volume of the box was adjusted to accommodate the water density to the experimental value for the temperature of interest: 0.997 g·cm^{-3} at 298 K and 0.829 g·cm^{-3} at 498 K (*28*, *29*). The solvent was then equilibrated by performing 1000 cycles of water minimization, followed by 1000 steps of MD and another 1000 cycles of minimization. Finally, the whole system was equilibrated by minimizing the protein for 1000 cycles and the protein plus solvent for 1000 cycles. After these preparation steps, initial atomic velocities were assigned from a Maxwellian distribution and periodically scaled until the target temperature (298 and 498 K) was reached. Classical MD simulations were performed in the NVE microcanonical ensemble, using a time step of 2 fs for integrating the equations of motion.

Each of the two simulations was carried out for 5 ns, saving structures for analysis every 0.2 ps. In all calculations, the nonbonded list was updated every five steps, and the nonbonded cutoff was 1 nm. In addition, two control simulations were performed at 298 and 498 K using the same protocol and with a nonbonded cutoff of 0.8 nm.

Materials. Azurin from *Pseudomonas aeruginosa* was obtained from Sigma Chemical Co. (St. Louis, MO). The purity was spectrophotometrically tested, and the absorbance ratio A_{625}/A_{280} was higher than 0.50. The protein was dissolved in 10 mM phosphate buffer, pH 7.02. Optical density (OD) and fluorescence measurements with a protein concentration of 0.4 mg/mL were carried out as previously described (*30*, *31*). In brief, OD was performed with a Jasco 7850 spectrophotometer equipped with a Peltier-type thermostated cell holder, using quartz cuvettes with a 1 cm optical path. Fluorescence was measured with a Perkin-Elmer LS 50B spectrofluorometer equipped with a Peltier temperature programmer PTP-1. The excitation wavelength was 295 nm, while the excitation and emission bandwidths were 6 and 4 nm, respectively.

CD measurements in the far-UV region were performed with a Jasco 810 spectropolarimeter equipped with a Peltier system using quartz cuvettes of 0.1 cm optical path. The azurin concentration was 0.3 mg/mL. Differential scanning calorimetry was performed on a VP-DSC (MicroCal Inc.) on a sample extensively degassed using a ThermoVac unit. At least five buffer−buffer runs were carried out in order to obtain a reproducible baseline before the protein scan. The protein concentration was 0.25 mg/mL.

In all experiments the temperature was scanned from 30 to 90 °C at a scan rate of 0.5 °C/min.

RESULTS AND DISCUSSION

MD simulations of azurin were performed for 5 ns at 298 and 498 K under the same conditions with the water density set to the experimental values. The room temperature simulation was provided as a control, and it was used for comparison as needed. At 298 K the protein remained nativelike, with C^{α} positional root mean square deviations (RMSD) of 0.30 ± 0.02 nm (Figure 2, gray line) with respect to the crystal structure. Visual inspection of protein snapshots (data not shown) at different simulation times showed that rearrangements were primarily localized to turns and loops, i.e., the most mobile regions, whereas the rest of the structure remained compact. In particular, the β-barrel maintained its topology and packing throughout the simulation. In contrast, at 498 K the RMSD of the C^{α} positions (Figure 2, black line) indicated that the unfolding process took place in less than 1 ns, since atomic deviation values of 1 nm are inconsistent with a fully folded structure.

Secondary Structure. Insight into the first steps of the unfolding process was obtained from the analysis of the protein secondary structure as a function of time. At room temperature the native hydrogen bond (HB) network was

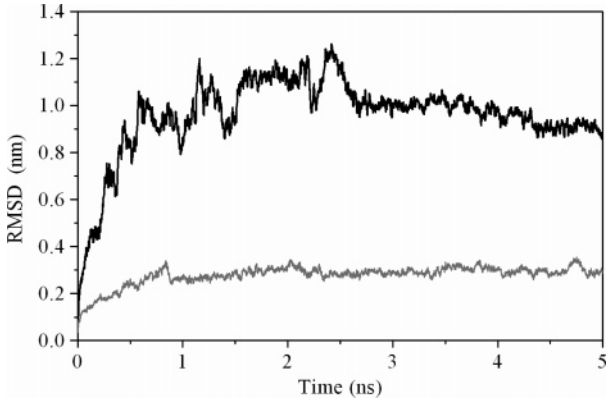

FIGURE 2: Root mean square deviations of C^{α} protein atoms from the crystal structure, at 298 K (gray line) and 498 K (black line), as a function of simulation time.

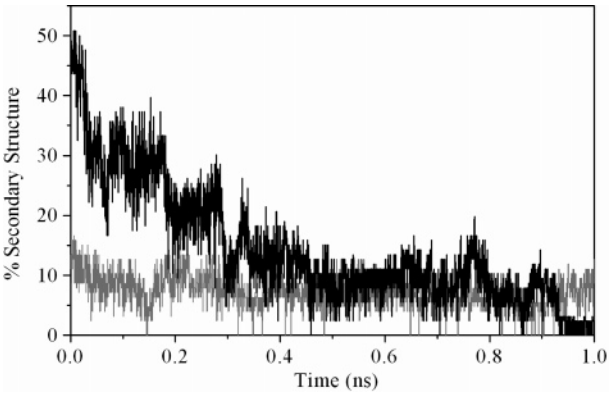

FIGURE 3: Percentage of α (gray line) and β (black line) secondary structure at 498 K as a function of simulation time.

retained during the simulation (data not shown). Figure 3 shows the percentage of α and β structure in the first nanosecond of simulation at 498 K. The amount of β structure, whose presence determines the folding topology of azurin, shows a clear decrease in the time interval 0−0.5 ns (black line). Two rough plateaus can be observed in the curve at about 0.1−0.2 and 0.2−0.3 ns, indicating transient dynamic conformations in which the protein moves further along the folding reaction coordinate without a substantial modification of the residual HB network arrangement of the main chain. In correspondence with the plateau at 0.2−0.3 ns, half of the β structure was still present (Figure 3, black line), as well as most of the α-helical structure (gray line). Disruption of the native β-structure assembly of azurin is not yet completed even after 0.5 ns, as 20−25% of the initial amount is still present. Total melting of this residual structure requires the protein to explore many more conformations, and a slow reduction is observed with time until full disappearance at 1 ns. α-Helical structure, on the other hand, seems to be more resistant to denaturation and dynamically forms and disappears throughout the simulation in many different unfolded structures of azurin (B. Rizzuti and V. Daggett, unpublished results).

Breakdown of the Hydrophobic Core. A key residue to monitor the unfolding of azurin both in simulation and in experiments is Trp48, which constitutes a natural probe to verify the exposure of the hydrophobic core. This residue is the only tryptophan in azurin, and in the native state it is buried in the interior region of the protein, shielded from the solvent. Therefore, fluorescence can be used as an

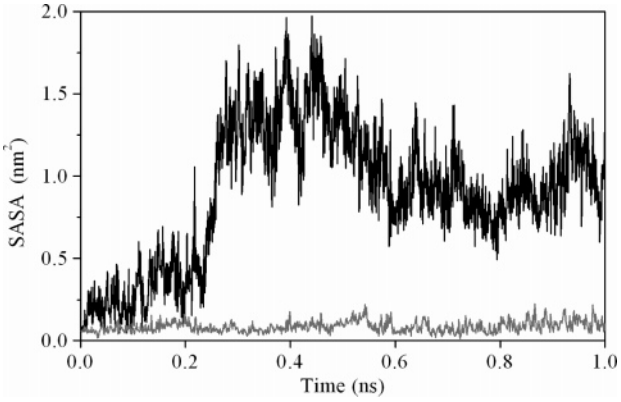

FIGURE 4: Solvent-accessible surface area (SASA) of the Trp48 residue, at 298 K (gray line) and 498 K (black line), as a function of simulation time.

experimental technique to monitor the disruption of the structure of azurin in aqueous solution under unfolding conditions. In Figure 4, solvent-accessible surface area (SASA) of the Trp48 side chain is reported as a function of simulation time. The curves show that at room temperature this residue remains buried in the protein core (gray line). At high temperature Trp48 becomes exposed to the solvent in the time interval 0.2−0.3 ns (black line). This result indicates that, at this stage, the unfolding process progresses by weakening the packing of the hydrophobic core. Water molecules penetrate into the protein scaffold, breaking the native tertiary contacts by competing to form HB and destabilizing the apolar interactions between residues. However, melting of the secondary structure (Figure 3) is yet to be completed when the tryptophan side chain becomes exposed to the solvent. As a consequence, hydration of the azurin core occurs while most of the β-strands maintain their native conformations.

Analysis of the native contacts between residues at different simulation times is able to elucidate structural details of the protein during the denaturation process. The overall results (data not shown) allow us to identify a defined mechanism for the exposition to the solvent of Trp48. In fact, in the first stages of the process the protein barrel was mostly preserved. Even though the β-strands tended to lose their nativelike twist, the peculiar face-to-face coordination of the two β-sheets was maintained. In contrast, the region formed by the α-helix and the following loop (which is approximately parallel to the helix and connects it to one of the two β-sheets; Figure 1a) moved away from the protein scaffold. This continuous movement propagated to the two adjacent strands 4 and 5 (Figure 1b) but not to the rest of the β-structure. In particular, Trp48 in the middle of the strand 4 pulled away from the β-barrel at this stage of the unfolding process. As a consequence of the separation of the α-helix from the rest of the protein, the side chain of Trp48 was extracted from inside the hydrophobic core, allowing water molecules to penetrate into the protein scaffold. Thus, exposure to the solvent of Trp48 preceded not only the melting of much of the secondary structure but also the complete disruption of the tertiary structure. This event substantially contributes to disruption of the native topology.

The Unfolding Process. The overall sequence of the early events in the simulated unfolding pathway of azurin is

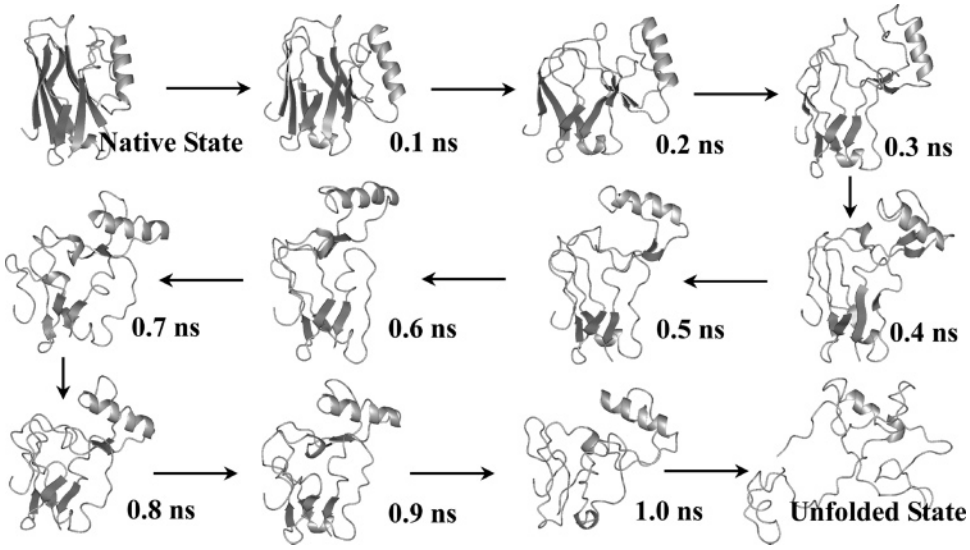

FIGURE 5: Snapshots of azurin structure at different simulation times at 498 K, representing the unfolding trajectory of the protein.

summarized in Figure 5, where snapshots of the protein at intervals of 0.1 ns are shown. In the first part of the trajectory (Figure 5, 0−0.5 ns), modifications were evident in the tertiary structure of azurin as a consequence of the flapping of the α-helix with respect to the rest of the protein. Simulations performed with different cutoffs for the nonbonded interactions (see Molecular Dynamics Simulations in the Materials and Methods section) and two additional runs with different initial atomic velocities all confirmed the same pathway for the disruption of the *β*-barrel in azurin. Therefore, on the basis of our simulation results, the Greek key motif in *β*-sheet B (Figure 1b) should form its native tertiary contacts only in the final steps of folding. It is possible that formation of this *β*-sheet is determined by short-range rather than long-range interactions, including perhaps the Cu ligands in the terminal *β*-hairpin (*32*). The Greek key motif contained in *β*-sheet A (Figure 1b), on the contrary, appears to be much more stable compared to the other sheet. In fact, the topology of strands 1−3 and 2b−8 was basically retained in the first nanosecond of simulation. In this respect, the unique disulfide bridge of azurin that connects the N-terminal portion of strands 1 and 3 seems to play a major role (*33*) by constraining the protein structure and preventing extensive exploration of conformational space.

After displacement of the α-helix with respect to the protein *β*-barrel, the subsequent part of the unfolding process (Figure 5, 0.5−1 ns) was characterized by massive penetration of water molecules into the protein scaffold. Tight interdigitation of side chains was lost, and the *β*-strands completely lost their nativelike twist. However, as a consequence of some hydrophobic clustering between the two *β*-sheets, the gross topology was retained. Retention of gross topology has been seen in MD simulations and confirmed in experiments also on barnase (*34*). Long-range ordering in a semicompact state may be a feature common to other proteins, as it would contribute to solve the Levinthal paradox by narrowing the conformational search in the folding process (*5*).

Finally, an unordered conformation of the protein chain was observed in the last part of the MD simulation (Figure 5, unfolded state), with highly dynamic tertiary interactions and some fluctuating helical structure. A propension was observed for the region encompassing residues 55−67 to partially re-form the native α-helix, thus fluctuating between a folded and unfolded state. The formation of small, dynamic hydrophobic clusters involving residues belonging to the native hydrophobic core was observed. This behavior, together with the presence of the disulfide bond that strongly constrains the protein structure in the N-terminus, contributes to prevent a sharp increase in C^{α} RMSD (Figure 2, black line). However, the complete loss of native *β* structure and topology allowed azurin to sample a wider conformational space. The protein was highly dynamic, with a continuous loss and formation of non-native tertiary contacts.

Comparison with Experiment. The results obtained in our simulations can be compared with the description of the unfolding process suggested by experiment. During the past years some of us (R. Guzzi and L. Sportelli) have employed several techniques to elucidate the thermal behavior of native azurin: optical density (OD), fluorescence, differential scanning calorimetry (DSC), far-UV circular dichroism (CD), and electron paramagnetic resonance (EPR). Such a variety of experimental data allows us to define a sequence of events describing the unfolding process as the temperature increases.

According to the experiments, exposure of Trp48, which is observed at an early stage in the simulations, constitutes the first event during the unfolding process of azurin. In fact, reduction of fluorescence intensity at $\lambda = 308$ nm is registered between 78 and 80 °C (351−353 K) (*31*). The fluorescence signal in azurin is due to Trp48, which is located in the hydrophobic core of the protein. Exposure of Trp48 to the aqueous solvent with high dielectric constant causes loss of the signal at 308 nm (Figure 6a, solid line) and a corresponding increase of emission at 357 nm (Figure 6a, dashed line). In the same temperature interval, 78−80 °C, the OD signal (Figure 6b) due to the $Cu-S_{Cys112}$ charge transfer transition begins to disappear (*11*, *35*). This effect could not be directly reproduced in our MD simulation, given the approximations in the modeling of the active site (classical mechanics is used to describe the motion of atoms, with constrained Cu−ligand bond distances). However, modifications in the $Cu-S_{Cys112}$ coordination were ascribed to structural rearrangement of the protein matrix (*30*). This is also supported by evidence that S_{Cys112} is a Cu ligand even

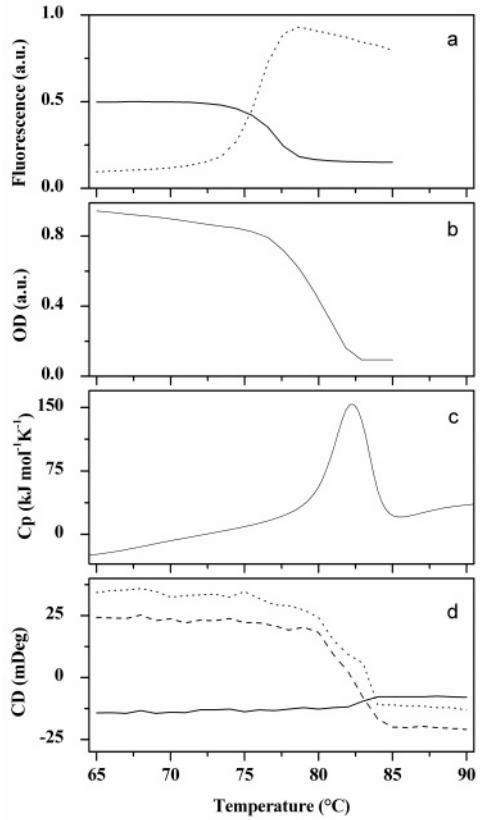

FIGURE 6: Unfolding of the azurin structure as a function of temperature, as monitored with different experimental techniques: (a) fluorescence, intensity at (solid line) $\lambda = 308$ nm and (dashed line) $\lambda = 357$ nm; (b) OD, normalized absorbance at $\lambda = 625$ nm; (c) DSC, heat capacity; (d) CD, band at (dotted line) 195 nm, distinctive of β-sheet, (dashed line) 200 nm, distinctive of unordered conformations (negative band, decrease in the curve indicates increase of random coil percentage), and (solid line) 222 nm, distinctive of α-helix (negative band, increase in the curve indicates decrease in the amount of helical structure).

in the unfolded state of azurin (*24*, *32*, *25*). Furthermore, EPR spectroscopy (*11*, *35*) reveals that the active site undergoes a conformational transition in the coordination of the Cu ion, which is another consequence of the reorganization of the tertiary structure (*36*). Our simulations indicate that the exposure of the hydrophobic core occurs simultaneously with alteration of the three-dimensional structure of the protein in the region around the active site. In fact, the two Cu ligand residues Gly45 and His46 are located at the beginning of β-strand 4 (Figure 1b), close to Trp48. Full extraction of Trp48 from the protein barrel necessarily requires displacement of these two residues with respect to the terminal β-hairpin formed by strands 7−8, which contains the other three Cu ligands.

At 80 °C (353 K) there is complete exposure of Trp48 to the solvent. The fluorescence curves approach their plateaus (minimum value for $\lambda = 308$ nm and maximum for $\lambda = 357$ nm), and the OD curve shows its midpoint (Figure 6a,b). These results indicate that, at this temperature, the hydrophobic core of azurin is disrupted. On the other hand, the C_p profile (Figure 6c) obtained by DSC (*11*) shows a low heat absorption below 80 °C, suggesting that the protein is at least partially intact. CD measurements were performed on native azurin in the amide region (190−260 nm) to monitor the melting of the secondary structure as a function of temperature. An accurate determination of the percentages of secondary structure is difficult because of the various contributions to the CD spectrum (twists of the β-sheets, length of the α-helices, presence of aromatic side chains, etc.) (*37*), and various methods can lead to different estimates (*38*). In Figure 6d the trend is reported for the main peaks in the CD spectra: the positive band at 195 nm (dotted line) distinctive of β-sheets (*39*), the negative band at 200 nm (dashed line) indicating a random coil conformation (*40*), and the negative band at 222 nm (solid line) corresponding to the $n \rightarrow \pi^*$ transition that characterizes α-helices. The curves indicate that a large degree of secondary structure is retained in azurin up to 80 °C. Consistent with experiment, our MD simulations show that solvation of the Trp48 side chain begins before full disruption of the tertiary structure, and it is completed before a total melting of the secondary structure. In particular, most of the β-barrel of azurin is still intact when the solvent starts to penetrate the protein core.

Finally, full unfolding of the protein structure occurs in the range of 80−86 °C (353−359 K), where far-UV CD data show a general melting of the secondary structure. As shown in Figure 6d, β structures dissolve (dotted line), and a corresponding decrease is observed in the curve representing the negative band at 200 nm (dashed line), indicating that the percentage of random coil increases. In the same temperature range, strong heat absorption is registered in the DSC curve (Figure 6c) with a peak at 84.4 °C, as further evidence of the disruption of the β-barrel of azurin. Comparison between the CD spectra (*30*) obtained after heating wild-type azurin up to 80 °C and after the DSC transition demonstrates that in this temperature interval the protein loses its secondary and tertiary structures that characterize the native folding topology. It is likely that it is only at this stage that the protein has enough energy to overcome the energy barrier separating the native and denatured states. Above the DSC transition temperature, experimental information is lacking.

CONCLUSIONS

Comparison with experiment is fundamental to validation of unfolding simulations at high temperature. In turn, simulations can reveal details of the unfolding process that are unobtainable by experimental techniques. In this work, the events characterizing the first steps of the unfolding pathway of azurin were monitored in MD as a function of simulation time and compared with the sequence of unfolding events occurring as a function of increasing temperature, as indicated by the experiments. The agreement between the simulation results and the experimental data is good. A picture emerges in which the unfolding of azurin begins with melting of some of the secondary structure, accompanied by alterations in the tertiary structure in the region of the helix. Disruption of the native topology of the β-barrel is driven by dislocation of the α-helix with respect to the protein scaffold. As a consequence, exposure to the solvent of the protein hydrophobic core and further disruptions of the tertiary structure around the active site occur. Both of these effects are also detected in experiments that use as molecular probes, respectively, the tryptophan residue (fluorescence) and the copper ion (EPR and OD). Only after this stage can the protein further progress toward the unfolded state, as also observed experimentally by DSC and CD.

ACKNOWLEDGMENT

B. Rizzuti is grateful to all of the members of the Daggett Research Group (Molecular Dynamics) for helpful discussions and warm hospitality in the Department of Medicinal Chemistry at the University of Washington, Seattle. The authors thank D. Milardi for the use of the CD equipment. MOLMOL (*41*) was used for the protein displays.

REFERENCES

1. Creighton, T. E. (1992) *Protein folding*, W. H. Freeman, New York.
2. Brockwell, D. J., Smith, D. A., and Radford, S. E. (2000) Protein folding mechanisms: new methods and emerging ideas, *Curr. Opin. Struct. Biol. 10*, 16−25.
3. Ferguson, N., and Fersht, A. R. (2003) Early events in protein folding, *Curr. Opin. Struct. Biol. 13*, 75−81.
4. Daggett, V. (2000) Long timescale simulations, *Curr. Opin. Struct. Biol. 10*, 160−164.
5. Daggett, V. (2002) Molecular dynamics simulations of the protein unfolding/folding reaction, *Acc. Chem. Res. 35*, 422−429.
6. Mayor, U., Johnson, C. M., Daggett, V., and Fersht, A. R. (2000) Protein folding and unfolding in microseconds to nanoseconds by experiment and simulation, *Proc. Natl. Acad. Sci. U.S.A. 97*, 13518−13522.
7. Mayor, U., Guydosh, N. R., Johnson, C. M., Grossman, J. G., Sato, S., Jas, G. S., Freund, S. M. V., Alonso, D. O. V., Daggett, V., and Fersht, A. R. (2003) The complete folding pathway of a protein from nanoseconds to microseconds, *Nature 421*, 863−867.
8. Ferguson, N., Pires, J. R., Toepert, F., Johnson, C. J., Pan, Y. P., Volkmer-Engert, R., Schneider-Mergener, J., Daggett, V., Oschkinat, H., and Fersht, A. R. (2001) Using flexible loop mimetics to extend Φ-value analysis to secondary structure interactions, *Proc. Natl. Acad. Sci. U.S.A. 98*, 13008−13013.
9. Day, R., Bennion, B. J., Ham, S., and Daggett, V. (2002) Increasing temperature accelerates protein unfolding without changing the pathway of unfolding, *J. Mol. Biol. 322*, 189−203.
10. Adman, E. T. (1991) Copper protein structures, *Adv. Protein Chem. 42*, 145−197.
11. La Rosa, C., Milardi, D., Grasso, D., Guzzi, R., and Sportelli, L. (1995) Thermodynamics of the thermal unfolding of azurin, *J. Phys. Chem. 99*, 14864−14870.
12. Arcangeli, C., Bizzarri, A. R., and Cannistraro, S. (1999) Long-term dynamics simulation of copper azurin: structure, dynamics and functionality, *Biophys. Chem. 78*, 247−257.
13. Luise, A., Falconi, M., and Desideri, A. (2000) Molecular dynamics simulation of solvated azurin: correlation between surface solvent accessibility and water residence times, *Proteins 39*, 56−67.
14. Rizzuti, B., Sportelli, L., and Guzzi, R. (2001) Evidence of reduced flexibility in disulfide bridge-depleted azurin: a molecular dynamics simulation study, *Biophys. Chem. 94*, 107−120.
15. Rizzuti, B., Swart, M., Sportelli, L., and Guzzi, R. (2004) Active site modeling in copper azurin molecular dynamics simulations, *J. Mol. Model. 10*, 25−31.
16. Nar, H., Messerschmidt, A., Huber, R., van de Kamp, M., and Canters, G. W. (1991) Crystal structure analysis of oxidized *Pseudomonas aeruginosa* azurin at pH 5.5 and pH 9.0. A pH-induced conformational transition involves a peptide bond flip, *J. Mol. Biol. 221*, 765−772.
17. van de Kamp, M., Canters, G. W., Wijmenga, S. S., Lommen, A., Hilbers, C. W., Nar, H., Messerschmidt, A., and Huber, R. (1992) Complete sequential ^{1}H and ^{15}N nuclear magnetic resonance assignment and solution secondary structure of the blue copper protein azurin from *Pseudomonas aeruginosa*, *Biochemistry 31*, 10194−10207.
18. Hoitink, C. W. G., Driscoll, P. C., Hill, H. A. O., and Canters, G. W. (1994) ^{1}H and ^{15}N nuclear magnetic resonance assignment, secondary structure in solution, and solvent exchange properties of azurin from *Alcaligenes denitrificans*, *Biochemistry 33*, 3560−3571.
19. Kalverda, A. P., Ubbink, M., Gilardi, G., Wijmenga, S. S., Crawford, A., Jeuken, L. J. C., and Canters, G. W. (1999) Backbone dynamics of azurin in solution: slow conformational change associated with deprotonation of histidine 35, *Biochemistry 38*, 12690−12697.
20. Levitt, M. (1990) ENCAD-Energy Calculations and Dynamics, Yeda, Rehovat, Israel.
21. Levitt, M., Hirshberg, M., Sharon, R., and Daggett, V. (1995) Potential energy function and parameters for simulations of the molecular-dynamics of proteins and nucleic-acids in solution, *Comput. Phys. Commun. 91*, 215−231.
22. Levitt, M., Hirshberg, M., Sharon, R., Laidig, K. E., and Daggett, V. (1997) Calibration and testing of a water model for simulation of the molecular dynamics of proteins and nucleic acids in solution, *J. Phys. Chem. B 101*, 5051−5061.
23. Sandberg, A., Leckner, J., Shi, Y., Schwarz, F. P., and Karlsson, B. G. (2002) Effects of metal ligation and oxygen on the reversibility of the thermal denaturation of *Pseudomonas aeruginosa* azurin, *Biochemistry 41*, 1060−1069.
24. De Beer, S., Wittung-Stafshede, P., Leckner, J., Karlsson, B. G., Winkler, J. R., Gray, H. B., Malmström, B. G., Solomon, E. I., Hedman, B., and Hodgson, K. O. (2000) X-ray absorption spectroscopy of folded and unfolded copper(I) azurin, *Inorg. Chim. Acta 297*, 278−282.
25. Pozdnyakova, I., Guidry, J., and Wittung-Stafshede, P. (2001) Probing copper ligands in denatured *Pseudomonas aeruginosa* azurin: unfolding His117Gly and His46Gly mutants, *J. Biol. Inorg. Chem. 6*, 182−188.
26. Marks, J., Pozdnyakova, I., Guidry, J., and Wittung-Stafshede, P. (2004) Methionine-121 coordination determines metal specificity in unfolded *Pseudomonas aeruginosa* azurin, *J. Biol. Inorg. Chem. 9*, 281−288.
27. Holm, R. H., Kennepohl, P., and Solomon, E. I. (1999) Structural and functional aspects of metal sites in biology, *Chem. Rev. 96*, 2239−2314.
28. Kell, G. S. (1967) Precise representation of volume properties of water at one atmosphere, *J. Chem. Eng. Data 12*, 66−69.
29. Haar, L., Gallagher, J. S., and Kell, G. S. (1984) NBS/NRC steam tables: thermodynamics and transport properties and computer programs for vapor and liquid states of water in SI units, Hemisphere Pub. Corp, Washington, DC.
30. Guzzi, R., Sportelli, L., La Rosa, C., Milardi, D., and Grasso, D. (1996) Experimental model for the thermal denaturation of azurin, *Biophys. Chem. 60*, 29−38.
31. Guzzi, R., Sportelli, L., La Rosa, C., Milardi, D., Grasso, D., Verbeet, M. P., and Canters, G. W. (1999) A spectroscopic and calorimetric investigation on the thermal stability of the Cys3Ala/Cys26Ala azurin mutant, *Biophys. J. 77*, 1052−1063.
32. Pozdnyakova, I., Guidry, J., and Wittung-Stafshede, P. (2000) Copper triggered β-hairpin formation. Initiation site for azurin folding?, *J. Am. Chem. Soc. 122*, 6337−6338.
33. Bonander, N., Leckner, J., Guo, H., Karlsson, B. G., and Sjölin, L. (2000) Crystal structure of the disulfide bond-deficient azurin mutant C3A/C26A. How important is the S−S bond for folding and stability?, *Eur. J. Biochem. 267*, 4511−4519.
34. Bond, C. J., Wong, K., Clarke, J., Fersht, A. R., and Daggett, V. (1997) Characterization of residual structure in the thermally denatured state of barnase by simulation and experiment: description of the folding pathway, *Proc. Natl. Acad. Sci. U.S.A. 94*, 13409−13413.
35. Guzzi, R., Sportelli, L., La Rosa, C., Milardi, D., and Grasso, D. (1998) Solvent isotope effect on azurin thermal unfolding, *J. Phys. Chem. B 102*, 1021−1028.
36. Bartucci, R., Guzzi, R., and Sportelli, L. (2001) Electron paramagnetic resonance investigation of biological systems, *Recent Res. Dev. Biophys. Chem. 2*, 85−101.
37. Johnson, W. C. (1999) Analyzing protein circular dichroism spectra for accurate secondary structure, *Proteins 35*, 307−312.
38. Greenfield, N. J. (1999) Applications of circular dichroism in protein and peptide analysis, *Trends Anal. Chem. 18*, 236−244.
39. Greenfield, N. J., and Fasman, G. D. (1969) Computed circular dichroism spectra for the evaluation of protein conformation, *Biochemistry 8*, 4108−4116.
40. Rodger, A., and Nordén, B. (1997) Circular dichroism and linear dichroism, Oxford University Press, Oxford.
41. Koradi, R., Billeter, M., and Wüthrich, K. (1996) *J. Mol. Graphics 14*, 51−55.

BI048685T